ACS OMEGA

http://pubs.acs.org/journal/acsodf

Article

Investigation on the Inhibition of Aluminum Dust Explosion by Sodium Bicarbonate and Its Solid Product Sodium Carbonate

Xiaokun Chen, Kunlun Lu,* Yang Xiao, Bin Su, Yuanyuan Wang, and Tenglong Zhao

Cite This: *ACS Omega* 2022, 7, 617−628

Read Online

ACCESS | Metrics & More | Article Recommendations

ABSTRACT: To characterize the inhibiting effects of sodium bicarbonate ($NaHCO_3$) on aluminum dust, the inhibiting capacities of $NaHCO_3$ and its solid product sodium carbonate (Na_2CO_3) on the explosions of 10 and 20 μm aluminum dusts were studied using a standard 20 L spherical chamber. Explosion parameters were analyzed based on the induction period and explosion stage to evaluate the inhibiting effects. The results show that the induction period of 10 μm aluminum dust explosion is 18.2 ms, which is shorter than that of 20 μm aluminum dust. Two aluminum dust explosions can be completely inhibited during the induction period when inert ratios of $NaHCO_3$ are 350 and 150%, respectively, but that is not observed after adding the corresponding amount of Na_2CO_3. When the inert ratio ranges from 0 to 150%, the physical effect of $NaHCO_3$ on 10 μm aluminum is poor and the chemical effect is the essential process. But as the inert ratio increased from 200% to 350%, the physical effect of $NaHCO_3$ is higher than the chemical effect, suggesting that the physical effect is the key factor. With the increase of $NaHCO_3$, the physical effect increases gradually. However, the chemical effect changes little. The physical effects of $NaHCO_3$ including heat absorption and isolation play an essential role in the inhibiting process, which has a significant impact on the pyrolysis process and explosion parameters. The results of the present work provide guidance for the prevention and control of aluminum dust explosions.

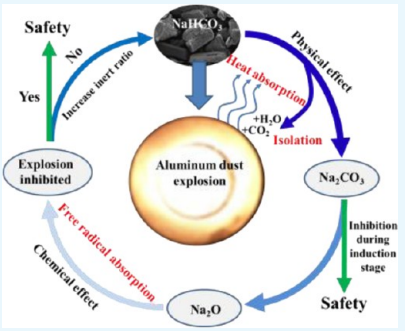

1. INTRODUCTION

In the aerospace field, metal fuels are superior to fossil fuels, because they provide a high energy density while being relatively nontoxic.[1,2] Aluminum dust is an attractive candidate of metal fuels, as the enthalpy of combustion of aluminum dust (84 kJ/cm^3) in oxygen is better than that of energetic materials and gaseous fuel. Aluminum dust was also widely used in other industries.[3] Many industrial processes generate aluminum dust, which is problematic because this material is highly combustible such that aluminum dust clouds can be readily ignited.[4−7] In fact, aluminum explosions have occurred in many countries to date, including the United States, Italy, and China.[8−10] As an example, in 2014, an especially large aluminum dust explosion took place at the Zhongrong Metal Products facility in Kunshan, China, causing 146 deaths and 163 injuries.[10,11] This hinders social progress and economic development and poses a great threat to individuals.[12,13] For these reasons, it is vital to develop better strategies for the mitigation and prevention of such explosions so as to allow the safe handling of aluminum dust.[14] Inhibition systems are an effective approach to mitigating accidental dust explosions.[15−18] In such systems, the inhibitor is sprayed into a restricted space immediately following the initiation of an explosion to prevent the expansion and propagation of the explosion. Numerous inhibitors have been developed and applied, such as phosphates,[19] alkali metal salts,[20−22] and ultrafine water mists,[23,24] each of which involves a different inhibiting function. Thus, it is important to investigate the interaction between a specific inhibitor and a combustible dust.

Sodium bicarbonate ($NaHCO_3$) has been used as an inhibitor because it exhibits superior performance based on physical and chemical effects.[25−35] Wang et al.[29] and Jiang et al.[30] studied the effects of $NaHCO_3$ powder on polyethylene dust and pulverized biomass dust explosions and demonstrated that the explosions could be completely suppressed by $NaHCO_3$. Dounia et al.[31] reported that $NaHCO_3$ particles decomposed in the flame front of premixed hydrocarbon/air, after which the resulting chemical reactions efficiently inhibited combustion. There also have been some works concerning the inhibition of aluminum dust explosion by $NaHCO_3$. Chen et al.[32] and Jiang et al.[33,34] monitored the explosion flame temperature and flame propagation behaviors of aluminum dusts inhibited by $NaHCO_3$, which have different particle size distributions. They found that the flame structures were changed by addition of $NaHCO_3$ and the size of the flame preheat zone was reduced accordingly. In summary, previous

Received: September 20, 2021
Accepted: December 22, 2021
Published: December 30, 2021

https://doi.org/10.1021/acsomega.1c05224
ACS Omega 2022, 7, 617−628

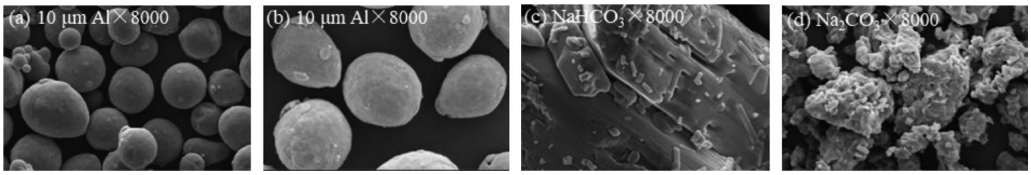

Figure 1. SEM of 10 and 20 μm aluminum dusts (a, b), $NaHCO_3$ (c), and Na_2CO_3 (d).

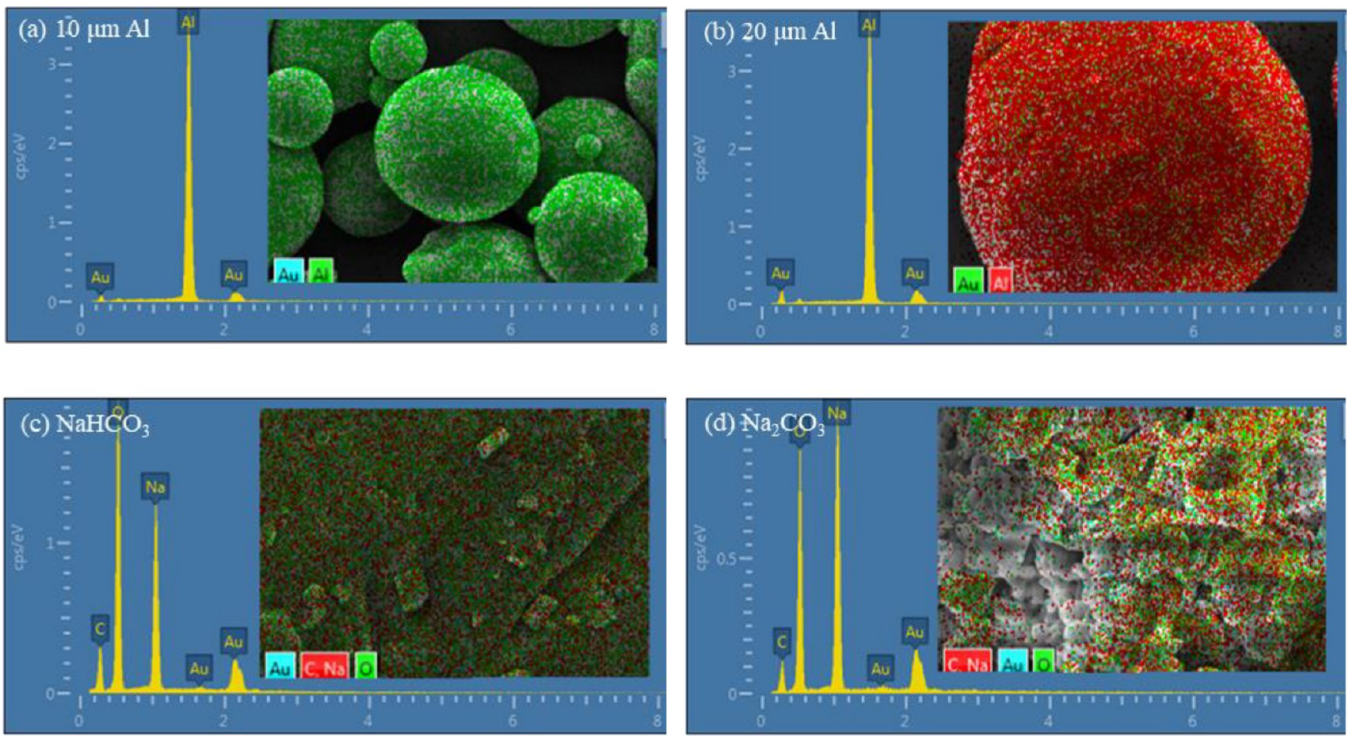

Figure 2. EDS of 10 and 20 μm aluminum dusts (a, b), $NaHCO_3$ (c), and Na_2CO_3 (d).

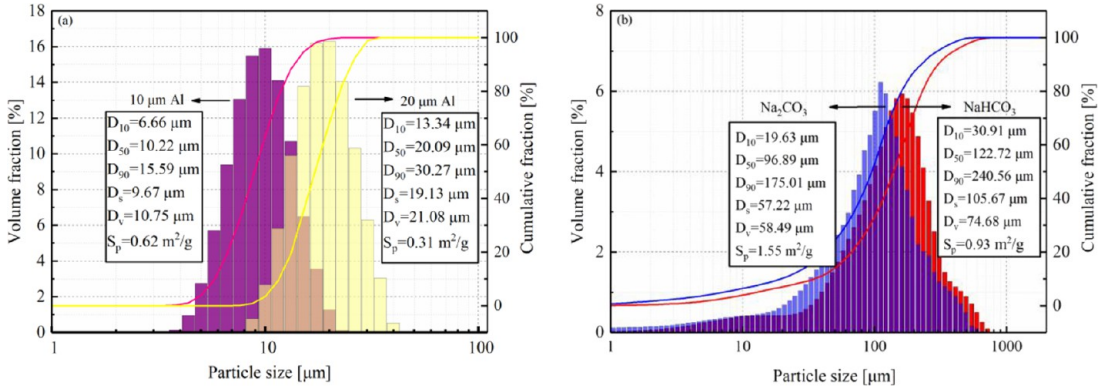

Figure 3. Particle size distribution of aluminum dusts (a) and $NaHCO_3$ and Na_2CO_3 (b).

studies showed that the inhibiting effects of $NaHCO_3$ included physical and chemical processes and the major research contents were focused on explosion parameters, flame propagation, and inhibition mechanism. They reported that the physical effect of $NaHCO_3$ was achieved by heat absorption and dilution, and the chemical effect was produced by sodium carbonate (Na_2CO_3), which is generated by $NaHCO_3$. However, a few studies focused on the inhibiting effects of $NaHCO_3$ and its solid product Na_2CO_3 on aluminum dust explosion to date. On the other hand, explosion parameters including the induction period and explosion pressure rising rate evolutions were also less studied. Therefore, further studies are needed to reveal the inhibiting effects of $NaHCO_3$ and its solid product Na_2CO_3 on aluminum dust explosion.

In this study, $NaHCO_3$ and its solid product Na_2CO_3 were adopted as suppressants to reveal physical and chemical effects of $NaHCO_3$ quantitatively. In addition, the control variable method was also used to evaluate the inhibiting effects of $NaHCO_3$ on aluminum dust explosion. The thermal decompositions and inhibiting effects of $NaHCO_3$ and Na_2CO_3 were conducted by a simultaneous thermal analyzer

https://doi.org/10.1021/acsomega.1c05224
ACS Omega 2022, 7, 617−628

(STA 449F3) and a 20 L spherical chamber, respectively. Furthermore, the characterizations for the physical and chemical effects of $NaHCO_3$ were studied during the induction period and explosion stage based on the explosion propagation characteristics and the micromorphology of explosive residues. The results of this work provide guidance for the prevention and control of aluminum dust explosions.

2. EXPERIMENT

2.1. Experimental Materials. Aluminum dust samples (10 and 20 μm) were obtained from Henan Yuanyang Powder Technology Co., Ltd. (Xinxiang, Henan Province, China). $NaHCO_3$ and Na_2CO_3 (analytically pure grade) were purchased from Sinopharm Chemical Reagent Co., Ltd. (Shanghai, China). The surface morphologies and chemical compositions of the aluminum samples, $NaHCO_3$, and Na_2CO_3 were analyzed using scanning electron microscopy with energy dispersive spectroscopy (SEM-EDS, FEC-450), and the results are shown in Figures 1 and 2. In addition, the particle size distributions of aluminum dusts, $NaHCO_3$, and Na_2CO_3 were determined by a Malvern Mastersizer 2000 laser particle size analyzer, adopting water and absolute alcohol as dispersants, as presented in Figure 3. The medium mean diameters, D_{50}, of aluminum dusts and $NaHCO_3$ and Na_2CO_3 powders are found to be 9.67, 19.13, 96.89, and 122.72 μm, respectively, and the specific surface areas of these four materials are 0.62, 0.31, 0.93, and 1.55 m^2/g, respectively. The elemental compositions of aluminum dusts are summarized in Table 1, and the results show that the aluminum contents of the two samples are 99.846 and 99.762%, respectively. Aluminum dusts, $NaHCO_3$, and Na_2CO_3 were dried at 50 °C in a vacuum oven for more than 6 h before the explosion tests.

Table 1. Elemental Composition of Aluminum Dusts

element	Al	Cu	Fe	Si
10 μm Al (%)	99.846	0.001	0.101	0.042
20 μm Al (%)	99.762	0.001	0.099	0.138

2.2. Experimental Apparatus. A diagram of the experimental device is shown in Figure 4. The device included a spherical test vessel, an ignition device, a control system, and a data acquisition system. The test vessel comprised a double-walled stainless steel sphere with a volume of 20 L and was attached to a 0.6 L dust container. The ignition device consisted of two spark rods and an ignition control panel that generated a discharge to ignite a 0.48 g charge made of zirconium powder, barium nitrate, and barium peroxide (4:3:3 by mass) that released 2 kJ of energy. The control system was used to input the desired ignition time and data acquisition time span, while the data acquisition system recorded pressure values throughout the trial.

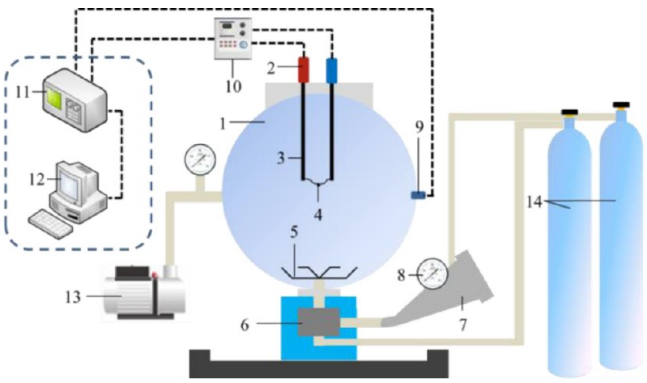

Figure 4. Dust explosion testing apparatus. 1, 20 L spherical test vessel; 2, electrode cap; 3, spark rod; 4, chemical igniter; 5, rebound nozzle; 6, outlet valve; 7, dust container; 8, pressure gauge; 9, pressure sensor; 10 and 11, control instrumentation; 12, computer; 13, vacuum pump; 14, compressed air tanks.

Prior to each trial, the preweighed portions of either aluminum powder, aluminum/$NaHCO_3$, or aluminum/Na_2CO_3 mixtures were transferred into the dust container of the test apparatus. After loading each sample into the spherical test vessel, the vessel was evacuated to a pressure of 0.06 MPa using a vacuum pump. Following this, aluminum dust was sprayed into the vessel by a flow of high-pressure air and ignited 60 ms later. The pressure and pressure rising rate in the vessel were recorded over time using a piezoelectric pressure sensor. The surface characteristics and chemical compositions of the solid residues were also examined using SEM-EDS. The ambient temperature and humidity were about 13−15 °C and 71−82%, respectively.

3. RESULTS AND DISCUSSION

3.1. Thermal Behaviors of $NaHCO_3$ and Na_2CO_3 Powders. The thermal behaviors of $NaHCO_3$ and Na_2CO_3 powders are essential in the inhibition process. The thermal behaviors of the samples were tested with the heating rate of 20 °C/min at the temperature range of 40−800 °C under the air atmosphere. Figure 5 shows the thermogravimetric-derivative thermogravimetric-differential scanning calorimetry (TG-DTG-DSC) curves of $NaHCO_3$ and Na_2CO_3 powders. It can be seen from Figure 5 that the decomposition of $NaHCO_3$ began at 140.0 °C and ended at 182.3 °C. During this stage, carbon dioxide (CO_2) and water vapor (H_2O) were generated by $NaHCO_3$, resulting in mass loss. Meanwhile, the mass loss of Na_2CO_3 began at 80.1 °C and ended at 101.3 °C due to the fact that water evaporated from it. The residual qualities of $NaHCO_3$ and Na_2CO_3 powders were 64.24 and 98.49%, respectively. Figure 5 shows that the DSC curves of $NaHCO_3$ and Na_2CO_3 had obvious endothermic peaks at 161.5 and 98.6 °C, respectively, and the areas of the endothermic peak of $NaHCO_3$ and Na_2CO_3 were 594.7 and 59.7 J/g, respectively. The findings indicate that heat absorption by $NaHCO_3$ is much higher than that by Na_2CO_3. Therefore, this is the obvious inhibiting difference between $NaHCO_3$ and its solid product Na_2CO_3 during the inhibition process.

The inhibiting effects of $NaHCO_3$ on aluminum dust explosion are not only heat absorption but also isolation and chemical inhibition,[29−35] and those of Na_2CO_3 contain isolation, chemical process, and little heat absorption. The heat absorbed by $NaHCO_3$ is much higher than Na_2CO_3 based on the DSC curves. In addition, the $NaHCO_3$ and Na_2CO_3 particles act as a physical barrier to reduce the collision probability of aluminum dust with an oxidant and also dilute the concentration of aluminum dust. The chemical effects of $NaHCO_3$ and Na_2CO_3 resulting from it are able to mitigate the explosion severity by generating sodium oxide and sodium hydroxide (NaOH) at high temperatures. NaOH is especially able to combine with H and OH free radicals during the explosion to interrupt the oxidation of aluminum[30−35] so that the chemical effects of $NaHCO_3$ and its solid product Na_2CO_3

https://doi.org/10.1021/acsomega.1c05224
ACS Omega 2022, 7, 617−628

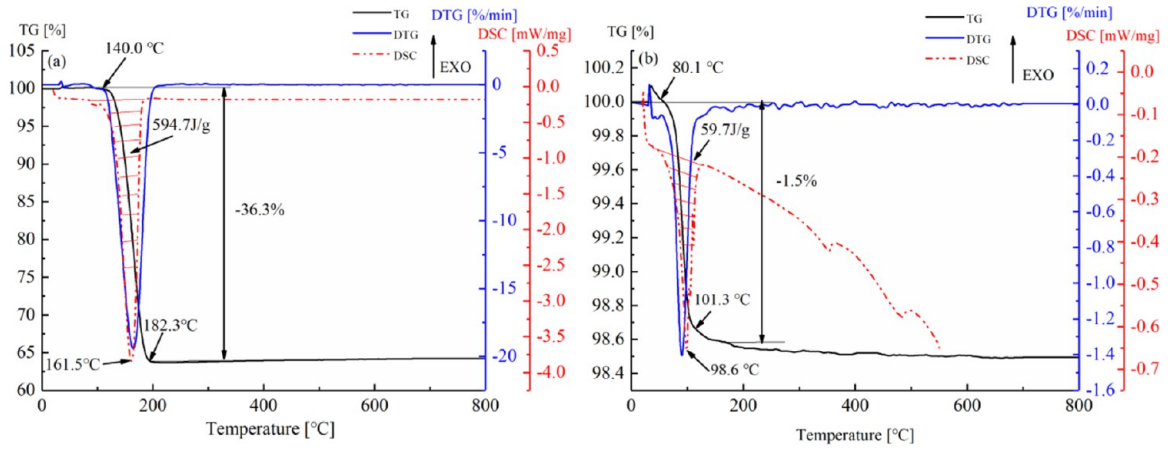

Figure 5. TG-DTG-DSC curves of $NaHCO_3$ (a) and Na_2CO_3 (b).

are similar under a certain ratio. During the analysis, it is reasonable to assume that $NaHCO_3$ is completely decomposed according to the thermal decomposition characteristics. Therefore, the different inhibiting effects between $NaHCO_3$ and its solid product Na_2CO_3 are heat absorption and dilution by CO_2 and H_2O under one certain ratio.

3.2. Typical Plots of 10 and 20 μm Aluminum Dust Explosions. The explosion characteristics of aluminum dusts are the basis of the inhibiting effect analysis. To ensure the analysis reliability, the aluminum dusts with different particle sizes including 10 and 20 μm were adopted in the present test. The typical plots of explosion pressure and pressure rising rate versus time of the two aluminum dust explosions at a concentration of 200 g/m^3 are shown in Figure 6. It can be

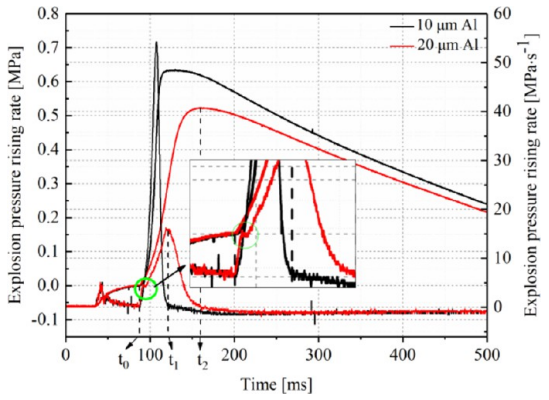

Figure 6. Pressure profiles obtained from aluminum dust explosions at 200 g/m^3.

seen from Figure 6 that each explosion pressure profile consists of an initial stage during which dust was injected into the test vessel, a second stage during which the pressure increased (corresponding to combustion of the aluminum), and a third stage associated with a decay in pressure. Also, the evolutions of pressure rising rate are consistent with explosion pressure profiles. The pressure rising rate first rises rapidly and then declines during the pressure rising stage and it remains constant in the pressure decay stage. The time of ignition, maximum pressure rising rate, and maximum explosion pressure were marked by t_0, t_1, and t_2, respectively, as shown in Figure 6. Hence, the pressure rising stage was divided into two parts by point t_1. The first part ranging from t_0 to t_1 is defined as the induction period, which belongs to the initial stage of explosion, and aluminum dusts decompose into smaller particles during this period. The induction periods of 10 and 20 μm aluminum dusts are 18.2 and 33.3 ms, respectively. Moreover, the second part from t_1 to t_2 is the violent explosion stage and the intense combustion occurs at the stage.

It must be emphasized that a characteristic inflection point appears after ignition on the pressure rising rate profiles of 20 μm aluminum dust but not observed on 10 μm aluminum dust as shown in Figure 6. The characteristic inflection point indicates that the pressure rising rate of 20 μm aluminum dust decreased in a few milliseconds after ignition. Aluminum dust is easily oxidized and forms an alumina shell on its surface.[36] After ignition, the oxide shell could burst and form aluminum vapor with a much smaller particle size, which reacts with oxygen, leading to explosion.[37,38] Owing to the fact that the particle size of 20 μm aluminum dust is larger than that of 10 μm aluminum dust, it needs much energy to melt the oxide shell, resulting in the pyrolysis of 20 μm aluminum dust, which is slower than that of 10 μm aluminum dust during the induction period. In addition, the change in aluminum dust particle size during explosion can be verified by the morphology of the explosion product as shown in Figure 7. It can be found from Figure 7 that the morphology of explosion residue is different from that of the raw dust as presented in Figure 1 and the particle size of the product changed much smaller after explosion. As presented in Figure 7, the particle size of explosion residue produced by 10 μm aluminum dust is smaller than that of 20 μm aluminum dust. Therefore, different pyrolysis of 10 and 20 μm aluminum dusts during the induction period leads to distinct explosion pressure and pressure rising rate. Also, the characteristic inflection point is important for the inhibition investigation and will be discussed later in this article.

From Figure 6, the maximum explosion pressure (P_m) values for 10 and 20 μm aluminum dusts were 0.64 and 0.52 MPa, respectively, while the maximum pressure rise rates ($(dP/dt)_m$) were 53.15 and 15.96 MPa/s. In each trial, the combustion time (t_c) was defined as the time from the point of ignition to the point at which P_m was obtained,[39,40] and the combustion times for the 10 and 20 μm specimens were 37 and 67 ms, respectively. The deflagration index (K_{st}) for each trial was calculated as[41−44]

https://doi.org/10.1021/acsomega.1c05224
ACS Omega 2022, 7, 617−628

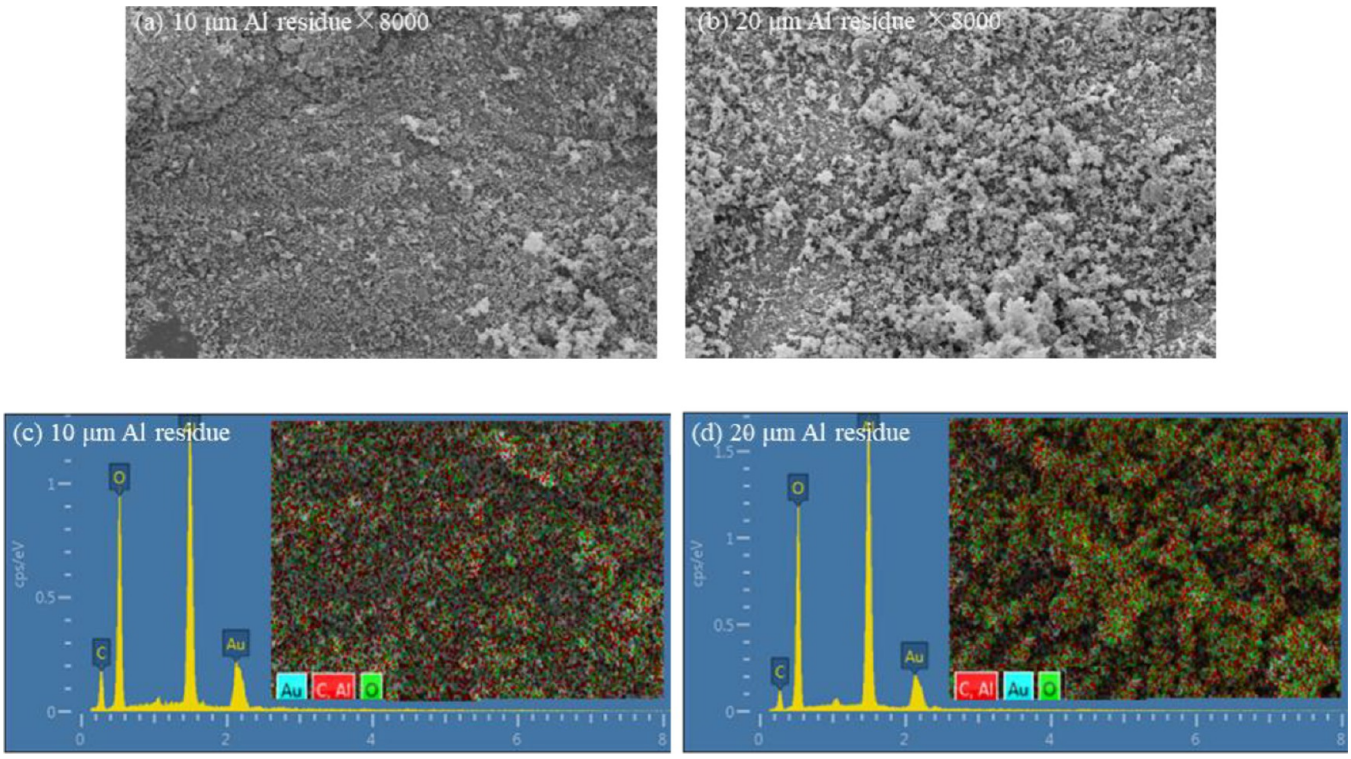

Figure 7. SEM (a, b) and EDS (c, d) of 10 and 20 μm aluminum dust explosion residues.

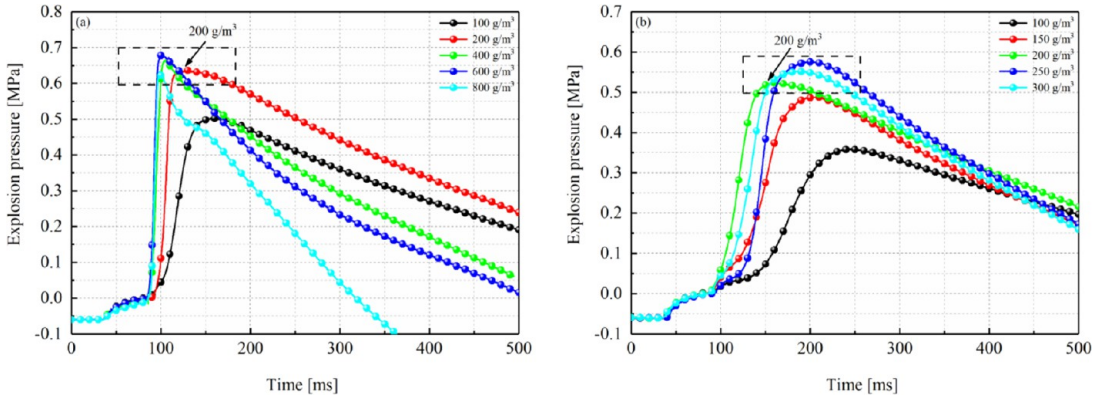

Figure 8. Explosion pressure curves of 10 μm (a) and 20 μm (b) aluminum dust explosions with various concentrations.

$$K_{st} = (dP/dt)_m \times V^{1/3} \quad (1)$$

where $(dP/dt)_m$ is the maximum rate of pressure rise (MPa/s) and V is the volume of the test vessel (m^3, V = 0.02 m^3 in the present work). The K_{st} values of 10 and 20 μm aluminum dusts were found to be 14.40 and 4.33 MPa·m/s in these tests, respectively. Furthermore, the explosion intensity of 10 and 20 μm aluminum dusts was studied under different concentrations, and the explosion pressure evolutions are shown in Figure 8. It can be seen that the P_m values increase first and then decrease both for 10 and 20 μm aluminum dust explosions. When the concentration of aluminum dust is higher than 200 g/m^3, the P_m values are almost close. Therefore, to ensure the complete decomposition of $NaHCO_3$ in the explosion process, 200 g/m^3 was adopted as the initial explosion concentration because the addition of $NaHCO_3$ will be increased and the complete decomposition of $NaHCO_3$ is difficult when the initial concentration of aluminum dust is high.

3.3. Explosion Parameters of Aluminum Dusts Mixed with $NaHCO_3$ and Its Solid Product Na_2CO_3.

The amount of aluminum used was equivalent to an aluminum dust concentration in the test vessel of 200 g/m^3. The inert ratio φ, equal to the mass of $NaHCO_3$ divided by the mass of aluminum dust, is used herein to indicate mass ratios in the test specimens. The inert ratio φ for each trial was calculated as

$$\varphi = \frac{M_{NaHCO_3}}{M_{Al}} \quad (2)$$

where φ is the inert ratio, and M_{NaHCO_3} and M_{Al} are the masses of $NaHCO_3$ and aluminum dust (g), respectively. The masses of Na_2CO_3 generated from various $NaHCO_3$ ratios are provided in Table 2.

3.3.1. Explosion Parameters of Aluminum/$NaHCO_3$ Mixtures. The inhibition experiments of 10 and 20 μm aluminum dust deflagration were conducted by a 20 L spherical chamber. Explosion pressure profiles of the

https://doi.org/10.1021/acsomega.1c05224
ACS Omega 2022, 7, 617−628

Table 2. Amounts of Na_2CO_3 Generated from $NaHCO_3$ at Various Ratios

inert ratio	50%	100%	150%	200%	250%	300%	350%
M_{NaHCO_3} (g)	2	4	6	8	10	12	14
$M_{Na_2CO_3}$ (g)	1.26	2.52	3.79	5.05	6.30	7.56	8.82

aluminum/$NaHCO_3$ mixtures are presented in Figure 9. It can be found that the aluminum dust explosions were changed by the addition of $NaHCO_3$. The pressure peaks gradually decreased as the inert ratio of $NaHCO_3$ increased from 50% to 350%. Especially, when the inert ratio was 350%, the P_m value of the mixture was 0.09 MPa, indicating that the explosion was completely inhibited by $NaHCO_3$. For 20 μm aluminum, the pressure peak disappeared and the explosion was suppressed when the inert ratio of $NaHCO_3$ was 150%. The results were obtained by the experiment, which provide guidance for the prevention and control of aluminum dust explosions by using $NaHCO_3$. It is noteworthy that the pressure rising rate evolutions are various under different inert ratios as presented in Figure 10. Figure 10a shows that the pressure rising rate of the 10 μm aluminum/$NaHCO_3$ mixtures increased rapidly during the induction period as the inert ratio ranged from 50 to 100%. However, when the inert ratio increased from 150% to 350%, the inflection points appeared on pressure rising rate profiles after ignition, indicating that the pyrolysis of 10 μm aluminum dust was slowed down by the addition of $NaHCO_3$. Figure 10b presents that the first inflection points appeared on pressure rising rate profiles of 20 μm aluminum dust when the inert ratio of $NaHCO_3$ was 50%. Therefore, these results show that the characteristic inflection point is a sign of inhibition and the inhibition process of $NaHCO_3$ can be described clearly by the explosion pressure rising rate evolution.

Figure 11 shows the explosion parameters including P_m, $(dP/dt)_m$, K_{st}, and t_c of 10 and 20 μm aluminum dusts mixed with various inert ratios of $NaHCO_3$. As the inert ratio was increased from 50% to 350%, the P_m values of the 10 μm aluminum/$NaHCO_3$ mixtures decreased from 0.63 MPa to 0.09 MPa, while the $(dP/dt)_m$ values of the mixtures decreased from 52.03 MPa/s to 4.8 MPa/s. Also, the t_c value increased from 38 ms to 72.8 ms during the 10 μm aluminum explosion as the ratio was increased over this same range. The K_{st} of the mixtures mixture was reduced from 13.88 MPa·m/s to 1.24 MPa·m/s. The explosion parameters of the 20 μm aluminum/$NaHCO_3$ mixtures show the same trend. These findings illustrate that the inhibition effect of $NaHCO_3$ on 20 μm aluminum dust is superior to that on 10 μm aluminum dust under a certain inert ratio. $NaHCO_3$ powder can absorb the heat of aluminum dust deflagration reactions, and the thermal decomposition of aluminum dust is insufficient. Due to the finding that 20 μm aluminum dust needs much energy to undergo pyrolysis, little heat loss will result in the explosion failure. The results indirectly suggest that the heat absorbed by $NaHCO_3$ has a significant impact on the evolution of pressure rising rate during the induction period.

3.3.2. Explosion Parameters of Aluminum/Na_2CO_3 Mixtures. $NaHCO_3$ could decompose into Na_2CO_3, CO_2, and H_2O at 140.0 to 182.3 °C. To qualitatively study the physical and chemical effects of $NaHCO_3$ on aluminum dust explosion, the effects of Na_2CO_3, which was generated by $NaHCO_3$, were also assessed. Figures 12 and 13 display the explosion pressure and pressure rising rate profiles of the aluminum/Na_2CO_3 mixtures. It can be noted that the pressure peak of 10 μm aluminum dust decreased slightly after the addition of Na_2CO_3. Especially, when the corresponding Na_2CO_3 at inert ratios of 350 and 150% was added, the explosions of 10 and 20 μm aluminum dusts were not suppressed by Na_2CO_3 and the pressure rising rate peaks of 10 and 20 μm aluminum dusts still exist. Figure 13a shows that the inflection point of 10 μm aluminum/Na_2CO_3 mixtures first appeared at an inert ratio of 200%, and it first appeared when 150% $NaHCO_3$ was added. These results indicate that the inhibiting effect of $NaHCO_3$ is better than that of Na_2CO_3 under a certain inert ratio both in the induction period and explosion stage.

Figure 14 plots the relationships between the inert ratio and P_m, $(dP/dt)_m$, K_{st}, and t_c. These data demonstrate that the addition of Na_2CO_3 reduced the explosion pressure of 10 μm aluminum dust by a little. Thus, the explosion pressure did not significantly decrease with increases in the concentration of Na_2CO_3, indicating that this compound had minimal additional effects as more was added to aluminum. Although there was only a slight reduction in the explosion pressure, the $(dP/dt)_m$ and K_{st} values were greatly lowered, while t_c was increased. The inhibiting effect of Na_2CO_3 on aluminum is primarily based on chemical inhibition, and any chemical reaction will be limited by the reactant present in the lowest stoichiometric amount.[30] In the present tests, the aluminum dust and air in the test vessel were the limiting reagents, and so, adding more Na_2CO_3 did not increase the chemical effect.

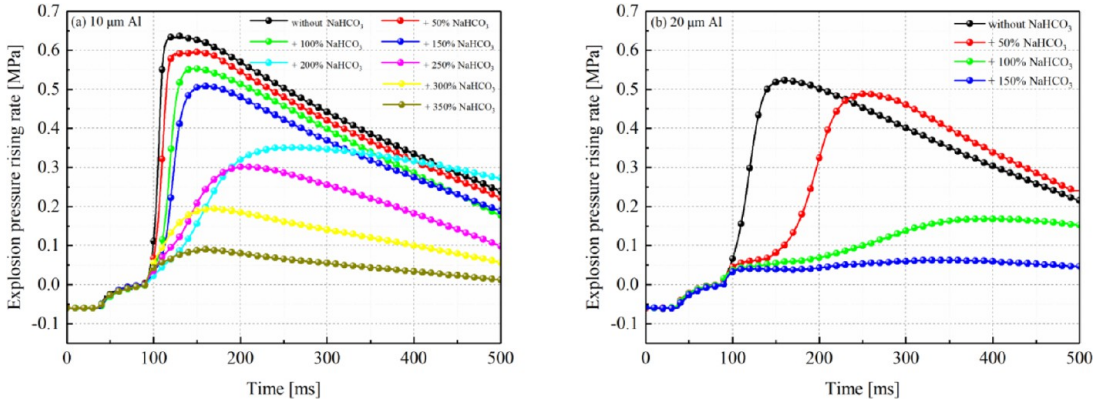

Figure 9. Explosion pressure profiles of 10 μm (a) and 20 μm (b) aluminum dusts mixed with $NaHCO_3$.

https://doi.org/10.1021/acsomega.1c05224
ACS Omega 2022, 7, 617−628

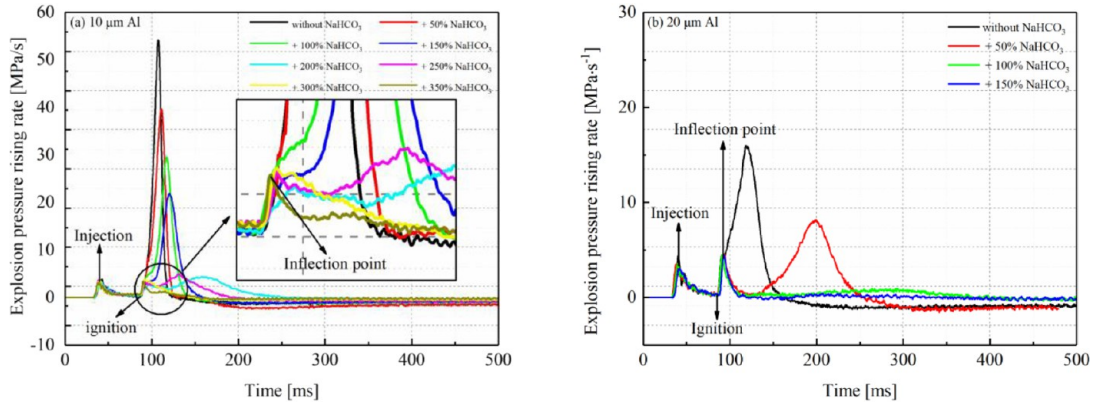

Figure 10. Explosion pressure rising rate profiles of 10 μm (a) and 20 μm (b) aluminum dusts mixed with $NaHCO_3$.

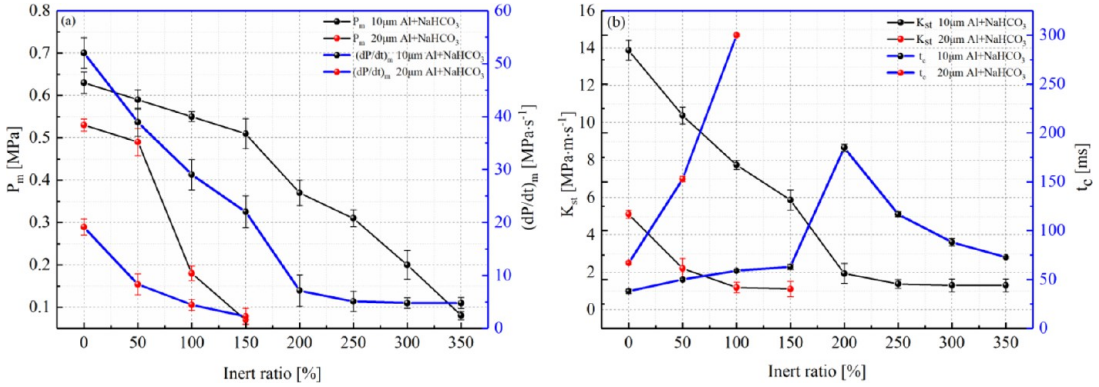

Figure 11. P_m and $(dP/dt)_m$ (a) and K_{st} and t_c (b) of aluminum/$NaHCO_3$ explosions.

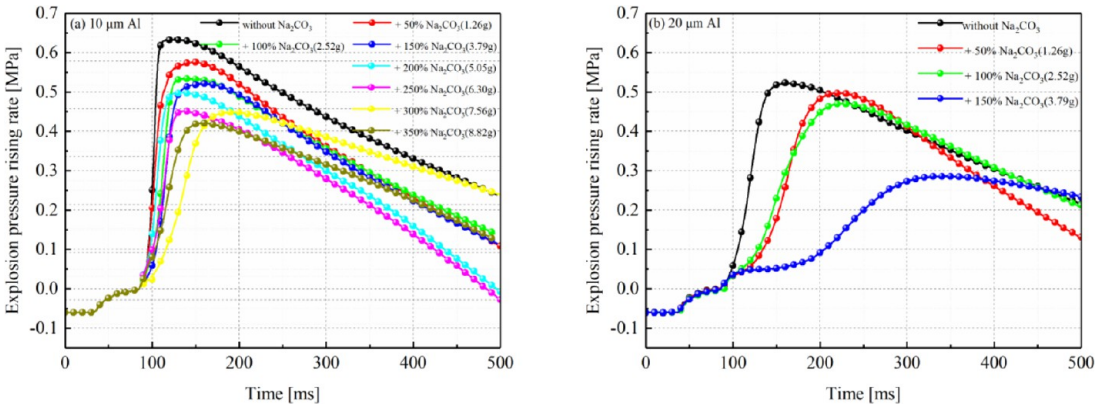

Figure 12. Explosion pressure profiles of 10 μm (a) and 20 μm (b) aluminum dusts mixed with Na_2CO_3.

3.4. Comparative Analysis Inhibition Effects of $NaHCO_3$ and Its Solid Product Na_2CO_3. *3.4.1. Inhibiting Effects of $NaHCO_3$ and Its Solid Product Na_2CO_3 on the Induction Period.* Based on the previous research results, the analysis of the inhibiting effects of $NaHCO_3$ and its solid product Na_2CO_3 on 10 and 20 μm aluminum dust explosions is discussed from two sides including the induction period and explosion stage. Figure 15 shows the induction period duration of aluminum dust explosion under various inert ratios of $NaHCO_3$ and the corresponding Na_2CO_3. It can be found that the induction period duration of 10 μm aluminum dust was prolonged as the inert ratio of $NaHCO_3$ increased from 0% to 350%. Especially, when the inert ratio was 350%, the induction period infinitely increased due to the finding that the pyrolysis of aluminum dust particles was a failure after ignition. However, when the corresponding Na_2CO_3 was added, the induction period duration increased slightly. Figure 15b shows that the induction period of 20 μm aluminum dust infinitely increased at an inert ratio of 150%. When the corresponding Na_2CO_3 was added, the induction period of aluminum/$NaHCO_3$ mixture was higher than that of aluminum/Na_2CO_3 mixture both for 10 and 20 μm aluminum dusts under a certain ratio. During the induction period, aluminum dust decomposed into small aluminum vapors, absorbing the energy released by the igniter. As $NaHCO_3$ was added, a lot of heat was absorbed, which resulted in the finding that the pyrolysis of aluminum dust was a failure. Due to the fact that 20 μm aluminum dust possesses a larger particle size, it needs more

https://doi.org/10.1021/acsomega.1c05224
ACS Omega 2022, 7, 617−628

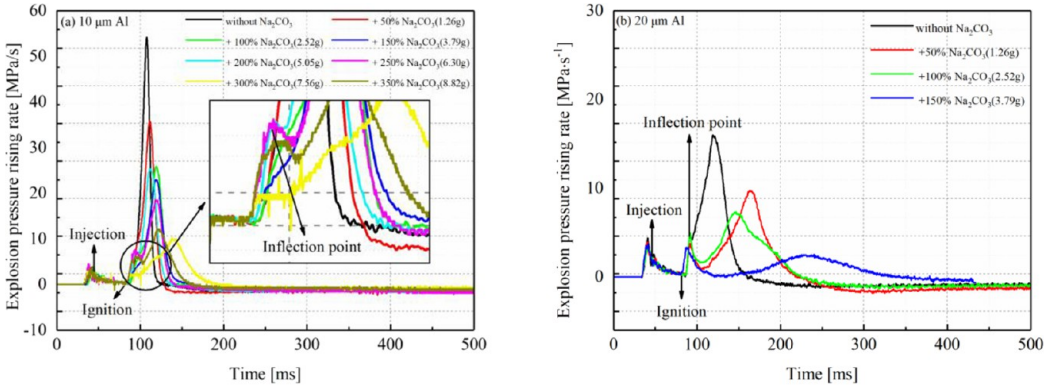

Figure 13. Pressure rising rate profiles of 10 μm (a) and 20 μm (b) aluminum dusts mixed with Na_2CO_3.

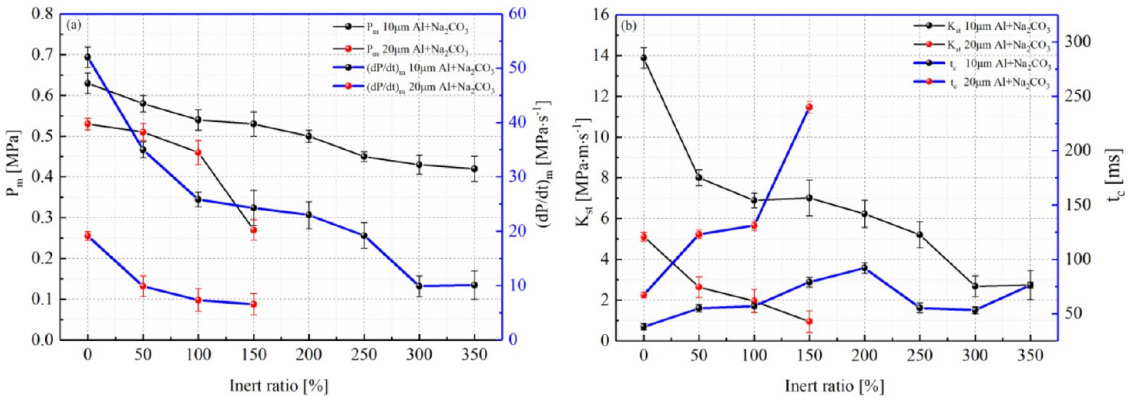

Figure 14. P_m and $(dP/dt)_m$ (a) and K_{st} and t_c (b) of aluminum/Na_2CO_3 explosions.

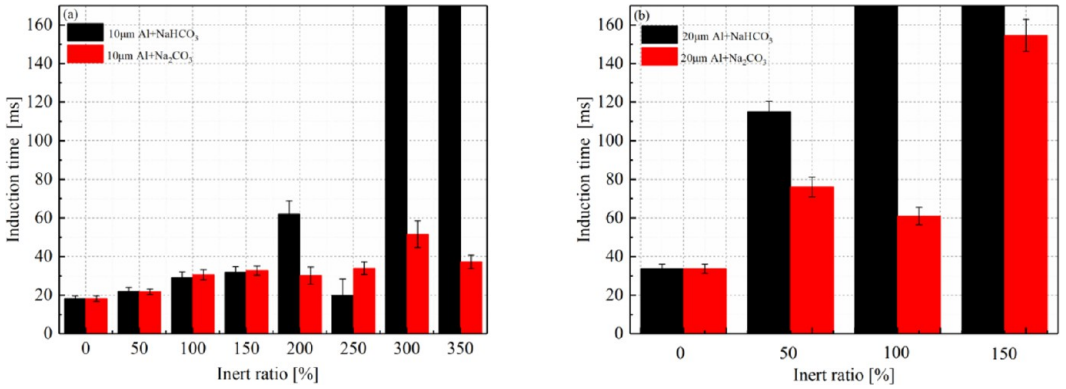

Figure 15. Induction period of 10 μm (a) and 20 μm (b) aluminum dusts mixed with $NaHCO_3$ and Na_2CO_3.

energy to achieve pyrolysis at the induction period. Therefore, little addition of $NaHCO_3$ could stop it from undergoing pyrolysis. On the contrary, 10 μm aluminum dust with a smaller particle size needs a larger amount of $NaHCO_3$ to achieve prevention. The flame propagation behavior can reflect the induction period more specifically as shown in Figure 16. Without addition of $NaHCO_3$, the initial flame of the explosion was very bright. However, with addition of $NaHCO_3$, the flame propagation gradually darkened. Especially, when 350 and 150% $NaHCO_3$ was added into 10 and 20 μm aluminum dusts, respectively, the chemical igniters flash and go out. Thus, these findings in this work suggest that the complete inhibition of aluminum dusts was realized during the induction period and the heat absorbed by $NaHCO_3$ is the essential effect in this process.

In addition, to verify the above conclusion, the microscopic features of explosion residues of aluminum/$NaHCO_3$ mixture at the inert ratio of 150% were tested as shown in Figures 17 and 18. Figure 17a shows that the shells and gaps of 10 μm aluminum particles were no longer present and large numbers of particle fragments were evident. However, it can be seen from Figure 17b that 20 μm aluminum dusts were still in the original shape and the surface of particles was covered with $NaHCO_3$, indicating that the pyrolysis of aluminum powder particles was a failure and combustion did not occur. In addition, the EDS of the explosion product shows that the main elements on the surface of 10 μm aluminum/$NaHCO_3$ explosion residue are aluminum (Al) and oxygen (O), while elements of 20 μm aluminum/$NaHCO_3$ explosion residue are O and sodium (Na). Furthermore, Figure 18b shows that the

https://doi.org/10.1021/acsomega.1c05224
ACS Omega 2022, 7, 617−628

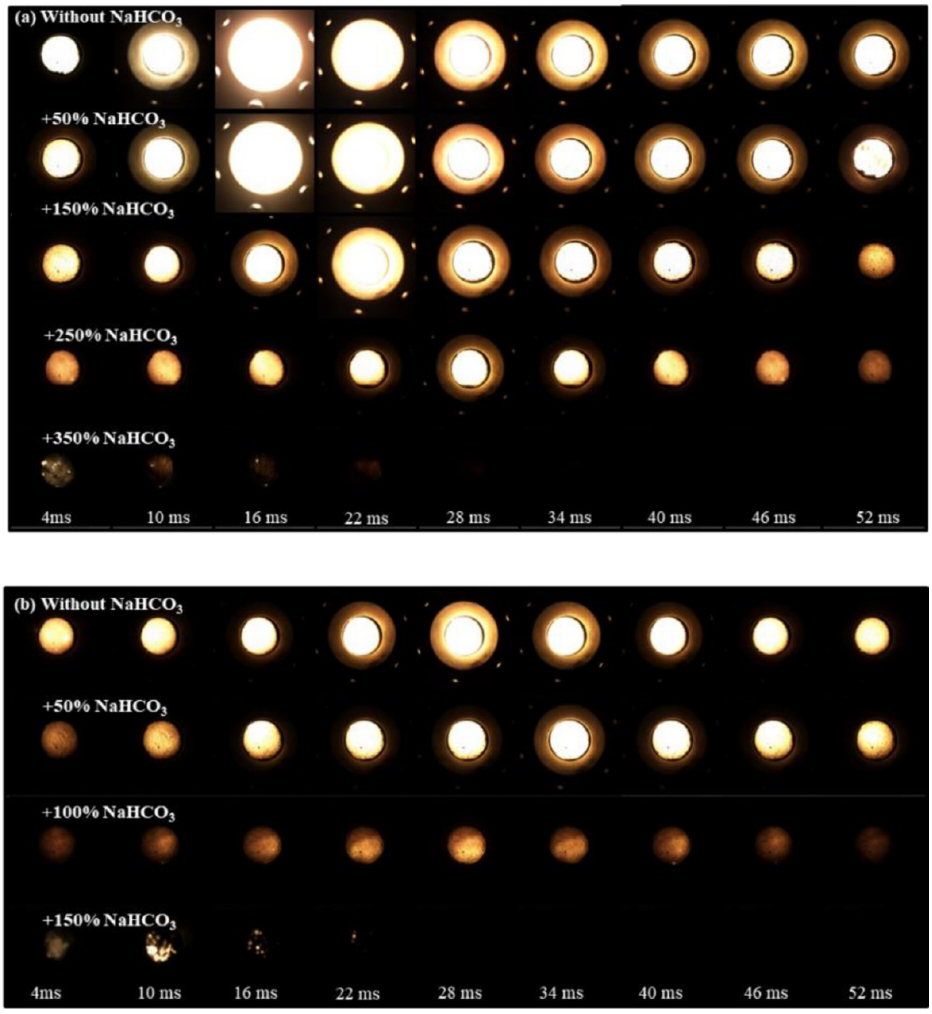

Figure 16. Flame propagations of 10 μm (a) and 20 μm (b) aluminum dusts mixed with $NaHCO_3$.

particle size distribution of residues was generally consistent with that of the original 20 μm aluminum particles, which means that the pyrolysis of aluminum dust was a failure. These distributions are also in agreement with the SEM images of residues as shown in Figure 17a,b. The findings provide evidence that the complete inhibition was achieved in the induction period and the pyrolysis was prevented by $NaHCO_3$.

3.4.2. Inhibiting Effects of $NaHCO_3$ and Its Solid Product Na_2CO_3 on the Explosion Stage. During the explosion stage, the reduction of P_m was used to evaluate the effect of $NaHCO_3$. Figure 19 shows the reduction of P_m and inhibiting rate of 10 and 20 μm aluminum dusts after the addition of $NaHCO_3$ and Na_2CO_3. As presented in Figure 19, the gray-marked part is the disparity of the inhibiting effect generated by $NaHCO_3$ and Na_2CO_3. According to previous discussion, the disparity of $NaHCO_3$ and Na_2CO_3 mainly contains a physical effect generated by $NaHCO_3$ including heat absorption and isolation due to the fact that they possess the same chemical effect. It is found that the gray-marked part increases with increasing inert ratio, indicating that the physical effect of $NaHCO_3$ increases. When the inert ratio ranges from 0 to 150%, the physical effect of $NaHCO_3$ on 10 μm aluminum is poor and the chemical effect is the essential process since it involves the chemical reaction between aluminum and $NaHCO_3$. As the inert ratio increased from 200% to 350%, the physical effect of $NaHCO_3$ is higher than the chemical effect, indicating that the physical effect is the key factor. When the inert ratio is 300%, the proportion of the physical effect of $NaHCO_3$ on 10 μm aluminum dust is 62%. As for 20 μm aluminum dust, the physical effect of $NaHCO_3$ worked efficiently at inert ratio ranges from 50 to 150%. Especially, when the inert ratio is 100%, the proportion of the physical effect of $NaHCO_3$ on 20 μm aluminum dust is 80%. On the other hand, the inhibition effect of Na_2CO_3 increased slowly due to the finding that the chemical effect was related to free radicals, whose concentration remained unchanged. The findings suggest that with the increase in $NaHCO_3$, the physical effect increased gradually, while the chemical effect changed little. In summary, the physical effect plays an important role in the aluminum dust explosion both for 10 and 20 μm aluminum dusts.

On the basis of the explosion parameters and microscopic features of explosion residues, the inhibition process of $NaHCO_3$ on aluminum dust was summarized as shown in Figure 20. It can be divided into two steps including the induction period and explosion stage. If the inert ratio of $NaHCO_3$ is higher than 350%, 10 μm aluminum dust can be inhibited completely during the induction period and the explosion stage cannot occur. During this period, the heat generated by the igniter was absorbed by $NaHCO_3$, leading to the failure of aluminum dust decomposition, suggesting that the physical effect plays a leading role. The inflection point on

https://doi.org/10.1021/acsomega.1c05224
ACS Omega 2022, 7, 617−628

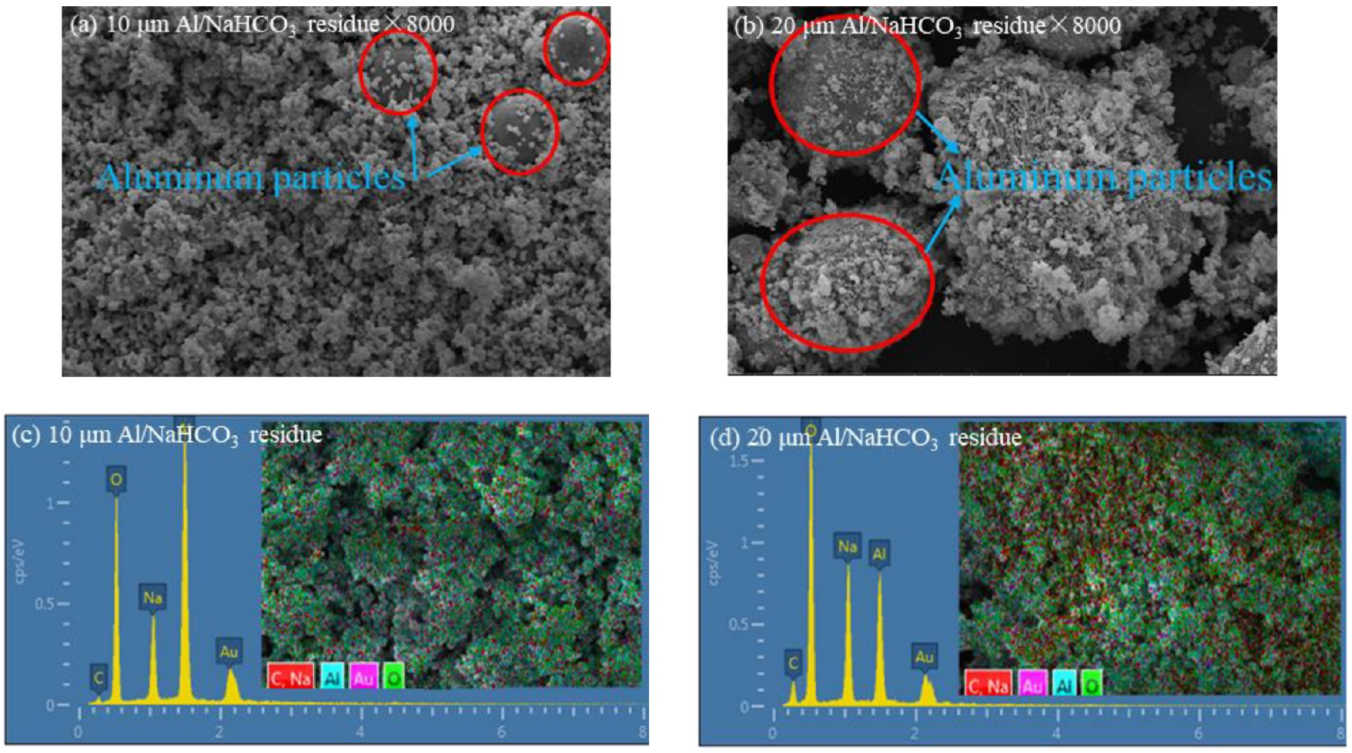

Figure 17. SEM (a, b) and EDS (c, d) of 10 and 20 μm aluminum/$NaHCO_3$ explosion residues.

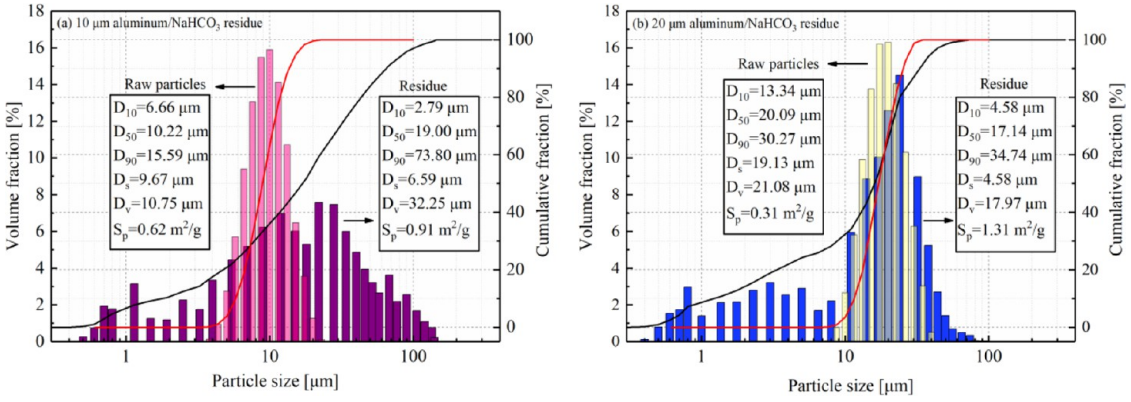

Figure 18. Particle size distributions of 10 μm (a) and 20 μm (b) aluminum/$NaHCO_3$ explosion residues.

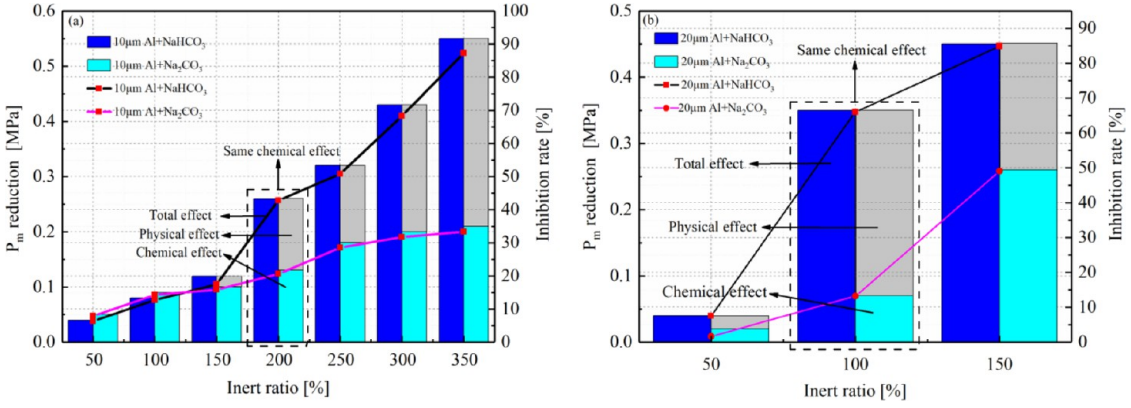

Figure 19. Reduction of P_m and inhibition rate of 10 μm (a) and 20 μm (b) aluminum mixed with $NaHCO_3$ and Na_2CO_3.

the pressure rising rate profiles is significantly characteristic of the inhibition process and it is also related to aluminum dust pyrolysis. When the inert ratio is lower than 350%, the inhibition process will fall into the explosion stage after the

https://doi.org/10.1021/acsomega.1c05224
ACS Omega 2022, 7, 617−628

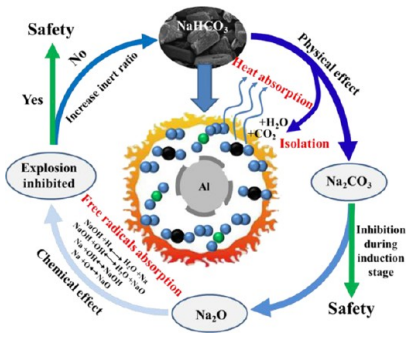

Figure 20. Inhibition process of $NaHCO_3$ on aluminum dust.

induction period. Under these circumstances, the physical and chemical effects will work together to decrease the P_m and $(dP/dt)_m$. Afterward, it needs to increase the inert ratio again to add in the system so that the inhibition process underwent a cycle once until the aluminum dust explosion was completed inhibited. All in all, the aluminum dust was completely inhibited by $NaHCO_3$ during the induction period and the physical effect plays a significant role in the inhibition process.

4. CONCLUSIONS

The inhibiting effects of $NaHCO_3$ and its solid product Na_2CO_3 on 10 and 20 μm aluminum dust explosions were investigated in a standard 20 L spherical chamber. The changes in induction period were revealed by pressure rising rate evolutions and the role of physical and chemical effects was illustrated by the reduction of P_m. The detailed conclusions of this work are as follows.

The inhibition process of $NaHCO_3$ can be described by the explosion pressure rising rate evolution. Based on the pressure rising rate evolution, the induction period of 10 μm aluminum dust explosion is 18.2 ms, which is shorter than that of 20 μm aluminum dust when the concentration of aluminum dust is 200 g/m^3. A large amount of heat was absorbed by $NaHCO_3$, causing the pyrolysis of 10 and 20 μm aluminum dusts to be a failure, and the explosion can be inhibited completely during the induction period when the inert ratios of $NaHCO_3$ are 350 and 150%, respectively. In addition, the characteristic inflection point on the pressure rising rate profiles is a sign of the pyrolysis of aluminum dust and it also can characterize the inhibiting process of the inhibitor.

The physical effects of $NaHCO_3$ including heat absorption and isolation play an essential role in the inhibiting process, which have a significant impact on aluminum dust pyrolysis and explosion parameters. With the increase of $NaHCO_3$, the physical effect increased gradually. However, the chemical effect changed little after the addition of the corresponding Na_2CO_3. When the inert ratio ranges from 0 to 150%, the physical effect of $NaHCO_3$ on 10 μm aluminum is poor and the chemical effect is the essential process. As the inert ratio increased from 200% to 350%, the physical effect of $NaHCO_3$ is higher than the chemical effect, suggesting that the physical effect is the key factor.

AUTHOR INFORMATION

Corresponding Author

Kunlun Lu − *College of Safety Science and Engineering, Xi'an University of Science and Technology, Xi'an, Shaanxi 710054, P.R. China; College of Chemistry and Environmental Engineering, Sichuan University of Science and Engineering, Zigong, Sichuan 643000, P.R. China;* orcid.org/0000-0003-3567-5051; Email: kunlun739@163.com

Authors

Xiaokun Chen − *College of Safety Science and Engineering, Xi'an University of Science and Technology, Xi'an, Shaanxi 710054, P.R. China*

Yang Xiao − *College of Safety Science and Engineering, Xi'an University of Science and Technology, Xi'an, Shaanxi 710054, P.R. China;* orcid.org/0000-0002-3960-9708

Bin Su − *College of Safety Science and Engineering, Xi'an University of Science and Technology, Xi'an, Shaanxi 710054, P.R. China*

Yuanyuan Wang − *College of Chemistry and Environmental Engineering, Sichuan University of Science and Engineering, Zigong, Sichuan 643000, P.R. China*

Tenglong Zhao − *College of Safety Science and Engineering, Xi'an University of Science and Technology, Xi'an, Shaanxi 710054, P.R. China*

Complete contact information is available at: https://pubs.acs.org/10.1021/acsomega.1c05224

Notes

The authors declare no competing financial interest.

ACKNOWLEDGMENTS

This study was supported by the National Key R&D Program of China (no. 2018YFC0807900). The authors also thank Henan Yuanyang Powder Technology Co., Ltd., of China for providing the experimental aluminum particles. The authors would like to thank Bin He from Shiyanjia Lab (www.shiyanjia.com) for the TG-DTG-DSC analysis.

REFERENCES

(1) Yu, X.; Yu, J.; Wang, C.; Lv, X.; Wang, Y.; Hou, Y.; Yan, X. Experimental study on the overpressure and flame propagation of hybrid hydrogen/aluminum dust explosions in a square closed vessel. *Fuel* **2021**, *285*, 119222.

(2) Vlaskin, M. S.; Shkolnikov, E. I.; Bersh, A. V.; Zhuk, A. Z.; Lisicyn, A. V.; Sorokovikov, A. I.; Pankina, Y. V. An experimental aluminum-fueled power plant. *J. Power Sources* **2011**, *196*, 8828−8835.

(3) Sundaram, D. S.; Puri, P.; Yang, V. A general theory of ignition and combustion of nano- and micron-sized aluminum particles. *Combust. Flame* **2016**, *169*, 94−109.

(4) Wang, Q.; Sun, Y.; Zhang, Z.; Shu, C.-M. Ignition and explosion characteristics of micron-scale aluminum-silicon alloy powder. *J. Loss Prev. Process Ind.* **2019**, *62*, 103940.

(5) Deng, J.; Qu, J.; Wang, Q.; Zhai, X.; Xiao, Y.; Cheng, Y.; Shu, C.-M. Minimum ignition temperature of aluminum dust clouds via the Godbert-Greenwald furnace. *Process Saf. Environ. Prot.* **2019**, *129*, 176−183.

(6) Wang, Q.; Fang, X.; Shu, C.-M.; Wang, Q.; Sheng, Y.; Jiang, J.; Sun, Y.; Sheng, Z. Minimum ignition temperatures and explosion characteristics of micron-sized aluminum powder. *J. Loss Prev. Process Ind.* **2020**, *64*, 104076.

(7) Li, H.; Deng, J.; Shu, C.-M.; Kuo, C.-H.; Yu, Y.; Hu, X. Flame behaviours and deflagration severities of aluminum powder-air mixture in a 20-L sphere: Computational fluid dynamics modelling and experimental validation. *Fuel* **2020**, *276*, 118028.

(8) Taveau, J.; Hochgreb, S.; Lemkowitz, S.; Roekaerts, D. Explosion hazards of aluminum finishing operations. *J. Loss Prev. Process Ind.* **2018**, *51*, 84−93.

(9) Marmo, L.; Piccinini, N.; Danzi, E. Small magnitude explosion of aluminum powder in an abatement plant: A telling cases. *Process Saf. Environ. Prot.* **2015**, *98*, 221−230.
(10) Li, G.; Yang, H.-X.; Yuan, C.-M.; Eckhoff, R. K. A catastrophic aluminum-alloy dust explosion in China. *J. Loss Prev. Process Ind.* **2016**, *39*, 121−130.
(11) Wang, X.; Wang, Z.; Ni, L.; Zhu, M.; Liu, C. Explosion characteristics of aluminum powder in different mixed gas environments. *Powder Technol.* **2020**, *369*, 53−71.
(12) Su, B.; Luo, Z.; Wang, T.; Zhang, J.; Cheng, F. Experimental and principal component analysis studies on minimum oxygen concentration of methane explosion. *Int. J. Hydrogen Energ.* **2020**, *45*, 12225−12235.
(13) Su, B.; Luo, Z.; Wang, T.; Xie, C.; Cheng, F. Chemical kinetic behaviors at the chain initiation stage of CH_4/H_2/air mixture. *J. Hazard. Mater.* **2021**, *403*, 123680.
(14) Taveau, J.; Vingerhoets, J.; Snoeys, J.; Going, J.; Farrell, T. Suppression of metal dust deflagrations. *J. Loss Prev. Process Ind.* **2015**, *36*, 244−251.
(15) Yang, J.; Li, Y.; Yu, Y.; Zhang, Q.; Zheng, L.; Suo, Y.; Jiang, J. Experimental investigation of the inerting effect of CO_2 on explosion characteristics of micron-size Acrylate Copolymer dust. *J. Loss Prev. Process Ind.* **2019**, *62*, 103979.
(16) Pei, B.; Yu, M. G.; Chen, L. W.; Wang, F. H.; Yang, Y.; Zhu, X. Experimental study on the synergistic inhibition effect of gas-liquid two phase medium on gas explosion. *J. Loss Prev. Process Ind.* **2017**, *49*, 797−804.
(17) Pei, B.; Yu, M.; Chen, L.; Zhu, X.; Yang, Y. Experimental study on the synergistic inhibition effect of nitrogen and ultrafine water mist on gas explosion in a vented duct. *J. Loss Prev. Process Ind.* **2016**, *40*, 546−553.
(18) Zhou, S.; Gao, J.; Luo, Z.; Hu, S.; Wang, L.; Wang, T. Role of ferromagnetic metal velvet and DC magnetic field on the explosion of a C_3H_8/air mixture-Effect on reaction mechanism. *Energy.* **2022**, *239*, 122218.
(19) Zhao, Q.; Chen, X.; Dai, H.; Huang, C.; Liu, J.; He, S.; Yuan, B.; Yang, P.; Zhu, H.; Liang, G.; Zhang, B. Inhibition of diammonium phosphate on the wheat dust explosion. *Powder Technol.* **2020**, *367*, 751−761.
(20) Wang, Q.; Sun, Y.; Jiang, J.; Deng, J.; Shu, C.-M.; Luo, Z.; Wang, Q. Inhibiting effects of gas-particle mixtures containing CO_2, $Mg(OH)_2$ particles, and $NH_4H_2PO_4$ particles on methane explosion in a 20-L closed vessel. *J. Loss Prev. Process Ind.* **2020**, *64*, 104082.
(21) Luo, Z.; Su, Y.; Chen, X.; Zheng, L. Effect of BC powder on hydrogen/methane/air premixed gas deflagration. *Fuel* **2019**, *257*, 16095.
(22) Bu, Y.; Li, C.; Amyotte, P.; Yuan, W.; Yuan, C.; Li, G. Moderation of Al dust explosions by micro- and nano-sized Al_2O_3 powder. *J. Hazard. Mater.* **2020**, *381*, 120968.
(23) Cao, X.; Ren, J.; Bi, M.; Zhou, Y.; Wang, Q. Experimental research on methane/air explosion inhibition using ultrafine water mist containing additive. *J. Loss Prev. Process Ind.* **2016**, *43*, 352−360.
(24) Liu, Z.; Zhong, X.; Zhang, Q.; Lu, C. Experimental study on using water mist containing potassium compounds to methane/air explosions. *J. Hazard. Mater.* **2020**, *394*, 122561.
(25) Kordylewski, W.; Amrogowicz, J. Comparison of $NaHCO_3$ and $NH_4H_2PO_4$ Effectiveness as Dust Explosion Suppressants. *Combust. Flame* **1992**, *90*, 344−345.
(26) Hamins, A. Flame extinction by sodium bicarbonate powder in a cup burner. *Symp. (Int.) Combust.* **1998**, *27*, 2857−2864.
(27) Going, J. E.; Snoeys, J. Explosion protection with metal dust fuels. *Process Safe Environ. Prot.* **2002**, *21*, 305−312.
(28) Birchall, J. D. On the mechanism of flame inhibition by alkali metal salts. *Combust. Flame* **1970**, *14*, 85−95.
(29) Wang, Y.; Lin, C. D.; Qi, Y. Q.; Pei, B.; Wang, L. Y.; Ji, W. T. Suppression of polyethylene dust explosion by sodium bicarbonate. *Powder Technol.* **2020**, *367*, 206−212.
(30) Jiang, H.; Bi, M.; Peng, Q.; Gao, W. Suppression of pulverized biomass dust explosion by $NaHCO_3$ and $NH_4H_2PO_4$. *Renewable Energy* **2020**, *147*, 2046−2055.
(31) Dounia, O.; Vermorel, O.; Poinsot, T. Theoretical analysis and simulation of methane/air flame inhibition by sodium bicarbonate particles. *Combust. Flame* **2018**, *193*, 313−326.
(32) Chen, X.; Zhang, H.; Chen, X.; Liu, X.; Niu, Y.; Zhang, Y.; Yuan, B. Effect of dust explosion suppression by sodium bicarbonate with different granulometric distribution. *J. Loss Prev. Process Ind.* **2017**, *49*, 905−911.
(33) Jiang, H.; Bi, M.; Gao, W.; Gan, B.; Zhang, D.; Zhang, Q. Inhibition of aluminum dust explosion by $NaHCO_3$ with different particle size distributions. *J. Hazard. Mater.* **2018**, *344*, 902−912.
(34) Jiang, H.; Bi, M.; Li, B.; Ma, D.; Gao, W. Flame inhibition of aluminum dust explosion by $NaHCO_3$ and $NH_4H_2PO_4$. *Combust. Flame* **2019**, *200*, 97−114.
(35) Yan, K.; Meng, X. An investigation on the aluminum dust explosion suppression efficiency and mechanism of a $NaHCO_3$/DE composite powder. *Adv. Powder Technol.* **2020**, *31*, 3246−3255.
(36) Li, Q.; Wang, K.; Zheng, Y.; Mei, N.; Lin, B. Explosion severity of micro-sized aluminum dust and its flame propagation properties in 20 L spherical vessel. *Powder Technol.* **2016**, *301*, 1299−1308.
(37) Li, Q.; Zhang, G.; Zheng, Y.; Liu, J.; Li, X. Investigation on the correlations between thermal behaviors and explosion severity of aluminum dust/air mixtures. *Powder Technol.* **2019**, *355*, 582−592.
(38) Millogo, M.; Bernard, S.; Gillard, P. Combustion characteristics of pure aluminum and aluminum alloys powders. *J. Loss Prev. Process Ind.* **2020**, *68*, 104270.
(39) Li, H.; Deng, J.; Chen, X.; Shu, C.-M.; Kuo, C.-H.; Hu, X. Influence of ignition delay on explosion severities of the methane-coal particle hybrid mixture at elevated injection pressures. *Powder Technol.* **2020**, *367*, 860−876.
(40) Jiang, H. P.; Bi, M. S.; Li, B.; Zhang, D. W.; Gao, W. Inhibition evaluation of ABC powder in aluminum dust explosion. *J. Hazard. Mater.* **2019**, *316*, 273−282.
(41) Li, H.; Deng, J.; Chen, X.; Shu, C.-M.; Kuo, C.-H.; Zhai, X.; Wang, Q.; Hu, X. Qualitative and quantitative characterisation for explosion severity and gaseous-solid residues during methane-coal particle hybrid explosions: An approach to estimating the safety degree for underground coal mines. *Process Safe Environ. Prot.* **2020**, *141*, 150−166.
(42) Ma, D.; Qin, B.; Gao, Y.; Jiang, J.; Feng, B. Study on the explosion characteristics of methane-air with coal dust originating from low-temperature oxidation of coal. *Fuel* **2020**, *260*, 116034.
(43) Luo, Z.; Li, R.; Wang, T.; Cheng, F.; Liu, Y.; Yu, Z.; Fan, S.; Zhu, X. Explosion pressure and flame characteristics of CO/CH_4/air mixtures at elevated initial temperatures. *Fuel* **2020**, *268*, 11737.
(44) Wang, T.; Luo, Z.; Wen, H.; Cheng, F.; Liu, L.; Su, Y.; Liu, C.; Zhao, J.; Deng, J.; Yu, M. The explosion enhancement of methane-air mixtures by ethylene in a confined chamber. *Energy* **2021**, *214*, 119042.

https://doi.org/10.1021/acsomega.1c05224
ACS Omega 2022, 7, 617−628